Instabilities of one-dimensional stationary solutions of the cubic nonlinear Schrödinger equation

Roger J. Thelwell†, John D. Carter‡, Bernard Deconinck†

†University of Washington
Department of Applied Mathematics
Seattle, WA 98195

‡Seattle University
Mathematics Department
Seattle, WA 98122

Draft - September 14, 2005

Abstract

We consider the two-dimensional cubic nonlinear Schrödinger (NLS) equation, which admits a large family of one-dimensional bounded traveling-wave solutions. All such stationary solutions may be written in terms of an amplitude and a phase. Solutions with piecewise constant phase have been well studied [19, 16, 11, 17]. **Although some solutions are stable under one-dimensional perturbations, no stable stationary solutions exist under two-dimensional perturbations [14, 5].** Here we consider stability of the larger class of solutions whose phase is dependent on the spatial dimension of the one-dimensional wave form. These solutions are said to have nontrivial-phase (NTP). We study the spectral stability of such NTP solutions numerically, using the spectrally based Hill's method. We present evidence which suggests that all such NTP solutions are unstable with respect to both one- and two-dimensional perturbations. Instability occurs in all cases: for both the elliptic and hyperbolic NLS equations, and in the focusing and defocusing case.

1 Introduction

The cubic nonlinear Schrödinger (NLS) equation in two spatial dimensions is given by

$$i\psi_t + \alpha\psi_{xx} + \beta\psi_{yy} + |\psi|^2\psi = 0. \tag{1}$$

The NLS equation is said be *focusing* or *attractive* in the x-dimension if $\alpha > 0$. If $\alpha < 0$, NLS is said to be *defocusing* or *repulsive* in the x-dimension. Similarly, the sign of β leads to focusing or defocusing in the y-dimension. The NLS equation is called *hyperbolic* if $\alpha\beta < 0$ and *elliptic* if $\alpha\beta > 0$.

Equation (1) admits a large family of one-dimensional bounded traveling-wave solutions. All such solutions, modulo Lie group symmetries [18], may be written in the form [4, 3]

$$\psi(x,t) = \phi(x)e^{i\theta(x)+i\lambda t}, \tag{2}$$

where $\phi(x)$ and $\theta(x)$ are real-valued functions, and λ is a real constant. Solutions of the form (2)

are possible if

$$\phi^2(x) = \alpha\left(-2k^2\,\mathrm{sn}^2(x,k) + B\right), \tag{3a}$$

$$\theta(x) = c\int_0^x \phi^{-2}(\xi)d\xi, \tag{3b}$$

$$\lambda = \frac{1}{2}\alpha(3B - 2(1+k^2)), \tag{3c}$$

$$c^2 = -\frac{\alpha^2}{2}B(B-2k^2)(B-2), \tag{3d}$$

where c is a real constant. Here $k \in [0,1]$ is the elliptic modulus of the Jacobi elliptic sine function, $\mathrm{sn}\,(x,k)$. The function $\mathrm{sn}\,(x,k)$ is periodic if $k \in [0,1)$, with period given by $L = 4K$, where $K = K(k)$ is defined by

$$K(k) = \int_0^{\pi/2} \left(1 - k^2\sin^2 x\right)^{-1/2}\,dx, \tag{4}$$

and is known as the complete elliptic integral of the first kind. When $k = 0$, $\mathrm{sn}\,(x,0) = \sin(x)$ with $L = 2\pi$. As k approaches 1, $\mathrm{sn}\,(x,k)$ approaches $\tanh(x)$ and L approaches infinity [2]. Although $\phi(x)$ inherits the periodicity of $\mathrm{sn}\,(x,k)$, the solution $\psi(x,t)$ is typically *not* L-periodic in the x-dimension, because the periods of $e^{i\theta}$ and ϕ are generally non-commensurate.

The solution ψ is said to have *trivial-phase* (TP) if $\theta(x)$ is (piecewise) constant and *nontrivial-phase* (NTP) if $\theta(x)$ is not constant. Equivalently, the solution ψ has TP if $c = 0$, and has NTP if $c \neq 0$. For every choice of α and β, (3) specifies a two-parameter family of NLS solutions in the free parameters k and B. Without loss of generality, we choose both α and β to be ± 1. The phase contribution $\theta(x)$ given in (3b) implicitly depends on α and B in both (3a) and (3d). In order for ϕ and θ to be real-valued functions, we need $B \in [2k^2, 2]$ if $\alpha = 1$ or $B \leq 0$ if $\alpha = -1$. Figure 1 includes the regions of (k,B)-parameter space that correspond to NTP solutions of the elliptic and hyperbolic NLS equations. As $c \to 0$, θ approaches a (piecewise) constant, and the NTP solutions reduce to one of five types of TP solutions: (*i*) a Stokes' plane wave, (*ii*) a cn-type solution, (*iii*) a dn-type solution, (*iv*) an sn-type solution, (*v*) a soliton-type solution. The limiting solutions correspond to boundaries of the regions in Fig. 1. Table 1 provides the values of k and B that cause (2) to limit to the TP solutions, and also gives the explicit expression for ψ in the TP limit. **The gray solitons, which are NTP solutions (not TP solutions), result when $k = 1$ and $B < 0$.** An overview of these NLS solutions is given in [4, 3]. Details of the Jacobi elliptic functions cn, dn and sn may be found in [2].

While both TP and NTP solutions are of interest, stability of TP solutions is well understood: for example, see [19, 16, 15, 9, 17, 8]. **While some TP solutions are stable under one-dimensional perturbations (the bright soliton [14] and sn-type solutions [5]), all TP solutions are known to be unstable under two-dimensional perturbations.** We know of only Infeld and Ziemkiewicz's paper [11] which considers the stability of NTP solutions of the NLS equation. **Results?**

The (k,B)-parameter space of TP solutions is essentially one-dimensional; it forms the boundary of the NTP (k,B)-parameter spaces shown in Fig. 1. The (k,B)-parameter space of the NTP solution is fully two-dimensional. **The large parameter space of the NTP setting, coupled with the fact that some TP solutions are stable with respect to some perturbations, gave hope that stable NTP solutions might exist.** f The more difficult linear stability

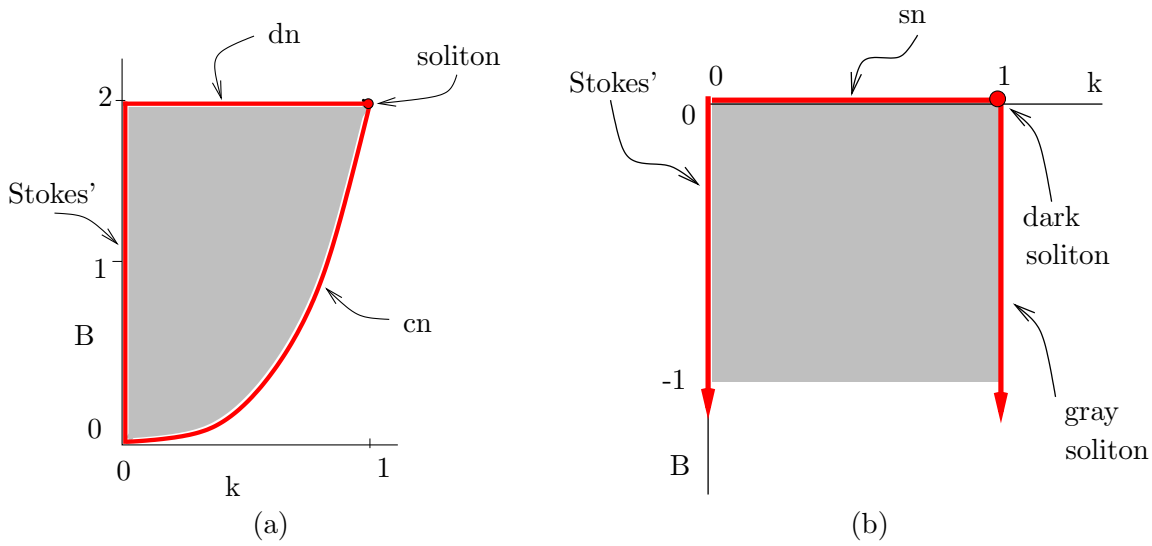

Figure 1: Admissible parameter space for solutions of the form given in (2) for (a) focusing ($\alpha = 1$) and (b) defocusing ($\alpha = -1$) regimes. The gray interior region corresponds to NTP solutions. The region in the defocusing regime is not bounded below.

problem and the large parameter space that needs to be explored makes the NTP setting more complex than the TP setting.

In this paper, we investigate the spectral stability of all NTP solutions (2), for all choices of $\alpha = \pm 1$ and $\beta = \pm 1$. That is, we compute the eigenvalues of an approximate spectral problem in order to identify possible growing modes in the linear stability problem. No spectrally stable NTP solutions were found, but the search did provide important stability information.

2 The linear stability problem

In order to study the linear stability of NTP solutions of the NLS equation, we consider perturbations of the form

$$\psi_p(x,y,t) = (\phi(x) + \epsilon u(x,y,t) + i\epsilon v(x,y,t) + \mathcal{O}(\epsilon^2))\, e^{i\theta(x)+i\lambda t}, \tag{5}$$

where $u(x,y,t)$ and $v(x,y,t)$ are real-valued functions, ϵ is a small real parameter and $\phi(x)\, e^{i\theta(x)+i\lambda t}$ is a NTP solution of NLS. Substituting (5) in (1), linearizing and separating real and imaginary parts leads to

$$\lambda u - 3\gamma\phi^2 u - \beta u_{yy} + \alpha c^2 \frac{1}{\phi^4} u - 2\alpha c \frac{1}{\phi^3}\phi_x v + 2\alpha c \frac{1}{\phi^2} v_x - \alpha u_{xx} = -v_t, \tag{6a}$$

$$\lambda v - \gamma\phi^2 v - \beta v_{yy} + \alpha c^2 \frac{1}{\phi^4} v + 2\alpha c \frac{1}{\phi^3}\phi_x u - 2\alpha c \frac{1}{\phi^2} u_x - \alpha v_{xx} = u_t. \tag{6b}$$

Since (6) does not depend on y or t explicitly, we may assume that $u(x,y,t)$ and $v(x,y,t)$ have the forms

$$u(x,y,t) = U(x,\rho,\Omega)\, e^{i\rho y+\Omega t} + c.c., \tag{7a}$$

	(k, B) value		Solution type	ψ
$\alpha = 1$	$k = 0$	$B \in [2k^2, 2]$	Stokes' plane wave	$\sqrt{B}\, e^{i(qx+\lambda t)}$
	$k \in (0, 1)$	$B = 2k^2$	cn-type	$\sqrt{2}\, k\, \mathrm{cn}\,(x, k)\, e^{i(2k^2-1)t}$
	$k \in (0, 1)$	$B = 2$	dn-type	$\sqrt{2}\, \mathrm{dn}\,(x, k)\, e^{i(2-k^2)t}$
	$k = 1$	$B = 2$	bright soliton	$\sqrt{2}\, \mathrm{sech}(x) e^{it}$
$\alpha = -1$	$k = 0$	$B \leq 0$	Stokes' plane wave	$\sqrt{B}\, e^{i(qx+\lambda t)}$
	$k \in (0, 1)$	$B = 0$	sn-type	$\sqrt{2}\, k\, \mathrm{sn}\,(x, k) e^{i(1+k^2)t}$
	$k = 1$	$B = 0$	dark soliton	$\sqrt{2}\, \tanh(x)\, e^{i2t}$

Table 1: Parameter values (k, B) which reduce NTP solutions to TP solutions. Here q is an arbitrary real constant.

$$v(x, y, t) = V(x, \rho, \Omega)\, e^{i\rho y + \Omega t} + c.c., \tag{7b}$$

where ρ is a real constant, $U(x)$ and $V(x)$ are complex-valued functions, Ω is a complex constant and *c.c.* denotes complex conjugate. Notice that ρ is the transverse wavenumber of the perturbation and Ω is the exponential growth rate associated with ρ. If bounded U, V exist such that Ω has a positive real part, then the amplitudes of the perturbations grow exponentially in time and the unperturbed solution is said to be unstable.

Upon substitution, (6) yields the spectral problem

$$\lambda U - 3\gamma\phi^2 U + \beta\rho^2 U + \alpha c^2 \frac{1}{\phi^4} U - 2\alpha c \frac{1}{\phi^3}\phi_x V + 2\alpha c \frac{1}{\phi^2} V_x - \alpha U_{xx} = -\Omega V, \tag{8a}$$

$$\lambda V - \gamma\phi^2 V + \beta\rho^2 V + \alpha c^2 \frac{1}{\phi^4} V + 2\alpha c \frac{1}{\phi^3}\phi_x U - 2\alpha c \frac{1}{\phi^2} U_x - \alpha V_{xx} = \Omega U. \tag{8b}$$

If $c = 0$, then (8) reduces to the stability analysis of TP solutions. This case is examined in [16, 11, 1, 13, 6, 5] and others. Using the linear system (8), we are now able to investigate the stability of the perturbed NTP solution numerically. We only consider the stability of NTP solutions in this paper.

3 Numerical investigation of spectral stability

The main difficulty for the numerical investigation of (8) is the size of the parameter space involved. For every choice of the equations parameters α, β and solution parameter pairs (k, B), the spectrum of (8) needs to computed for a range of ρ values in order to determine stability or to analyze any instabilities. An efficient numerical method is necessary. Hill's method [7], which exhibits exponential convergence, allows for the systematic exploration of the large phase space encountered here.

3.1 Hill's method

To apply Hill's method, Fourier expansions are needed for all coefficients of (8). Using the complex Fourier form, we have

$$\begin{aligned} \phi^2(x) &= \sum_{n=-\infty}^{\infty} Q_n e^{i2n\pi x/L}, & \phi^{-2}(x) &= \sum_{n=-\infty}^{\infty} R_n e^{i2n\pi x/L}, \\ \phi^{-4}(x) &= \sum_{n=-\infty}^{\infty} S_n e^{i2n\pi x/L}, & \phi^{-3}(x)\phi'(x) &= \sum_{n=-\infty}^{\infty} T_n e^{i2n\pi x/L}, \end{aligned} \tag{9}$$

where Q_n, R_n, S_n and T_n are the Fourier coefficients. Note that $\phi^2(x)$ has period $L/2$ and that $\phi(x)$ is never zero except in the TP limit cases.

The periodicity of the coefficients in (8) allows us to decompose the eigenfunction components U and V of (8) in a Fourier-Floquet form

$$U(x) = e^{i\mu x} \sum_{n=-\infty}^{\infty} U_n e^{in\pi x/L} \quad \text{and} \quad V(x) = e^{i\mu x} \sum_{n=-\infty}^{\infty} V_n e^{in\pi x/L}. \tag{10}$$

The form of U and V in (10) follows from Floquet's theorem and the observation that we seek eigenfunctions, which are bounded by definition. This decomposition has the benefit of admitting both L-periodic and L-anti-periodic eigenfunctions when $\mu = 0$. Recall that ψ is typically only quasiperiodic. Allowing μ to be different from 0 gives rise to solutions that are either quasiperiodic or have period greater than L.

Substitution of (9) and (10) into (8) and equating Fourier coefficients allows us to write equations for U_n and V_n as a coupled bi-infinite system of difference equations given by

$$\begin{aligned} -\left(\lambda + \beta\rho^2 - \alpha\left(i\mu + \frac{in\pi}{L}\right)^2\right) U_n + 3\gamma \sum_{m=-\infty}^{\infty} Q_{\frac{n-m}{2}} U_m - \alpha c^2 \sum_{m=-\infty}^{\infty} S_{\frac{n-m}{2}} U_m \\ + 2\alpha c \sum_{m=-\infty}^{\infty} T_{\frac{n-m}{2}} V_m - 2\alpha c\left(i\mu + \frac{in\pi}{L}\right) \sum_{m=-\infty}^{\infty} R_{\frac{n-m}{2}} V_m = \Omega V_n, \end{aligned} \tag{11a}$$

$$\begin{aligned} \left(\lambda + \beta\rho^2 - \alpha\left(i\mu + \frac{in\pi}{L}\right)^2\right) V_n - \gamma \sum_{m=-\infty}^{\infty} Q_{\frac{n-m}{2}} V_m + \alpha c^2 \sum_{m=-\infty}^{\infty} S_{\frac{n-m}{2}} V_m \\ + 2\alpha c \sum_{m=-\infty}^{\infty} T_{\frac{n-m}{2}} U_m - 2\alpha c\left(i\mu + \frac{in\pi}{L}\right) \sum_{m=-\infty}^{\infty} R_{\frac{n-m}{2}} U_m = \Omega U_n, \end{aligned} \tag{11b}$$

for all integers n. The system of equations (11) is *equivalent* to the original system (8). Here $\mu \in [\frac{-\pi}{K}, \frac{\pi}{K})$ and $Q_{\frac{n-m}{2}} = 0$ if $\frac{n-m}{2} \notin \mathbb{Z}$, with $R_{(\cdot)}, S_{(\cdot)}$ and $T_{(\cdot)}$ defined similarly.

In practice, a pre-multiplication of the linear system by ϕ^4 allows for the exact cosine series expansion of ϕ^2, ϕ^4 and ϕ^6 to be used. This follows from the differential equations for $\mathrm{sn}\,(x,k)$ and Jacobi's series expansion of $\mathrm{sn}^2(x,k)$ [12]. This pre-multiplication transforms the original eigenvalue problem into a generalized eigenvalue problem [10].

Parameter	Description	Value
k	Elliptic modulus	$\texttt{linspace(0,1,65)}$
B	Shift	For $\alpha = -1$: $-\texttt{logspace}(-8,0,65)$ For $\alpha = \ \ 1$: $(2k^2 + \texttt{logspace}(-8,0,65)) \cap (2k^2, 2)$
N	Fourier cutoff	For $\alpha = -1$: $15 + \texttt{ceil}(5\texttt{k}^5)$ For $\alpha = \ \ 1$: $10 + \texttt{ceil}(25\texttt{k}^{10})$
ρ	Perturbation wavenumber	$\texttt{linspace(0,4,65)}$
μ	Floquet parameter	$\texttt{linspace}(-\frac{\pi}{\texttt{K}}, \frac{\pi}{\texttt{K}}, 21)$

Table 2: Parameter values and ranges used in numerical experiments. Only perturbed NTP solutions are considered.

3.2 Numerical experiments

By choosing a finite number of Fourier modes, the exact bi-infinite system (11) is truncated. We explicitly construct and compute approximations to the spectral elements of (8) by finding the eigenvalues of the truncated version of (11). We consider all four cases individually: (I) focusing in both x and y ($\alpha = \beta = 1$), (II) focusing in x and defocusing in y ($\alpha = -\beta = 1$), (III) defocusing in x and focusing in y ($-\alpha = \beta = 1$) and finally, (IV) defocusing in both x and y ($-\alpha = -\beta = 1$).

In each case, a large number of parameter values in the two-dimensional parameter space shown in Fig. 1 were explored numerically. The (k, B)-parameter values considered correspond to fully NTP solutions, and do not include TP solutions. Approximately 5.2 million generalized eigenvalue problems were considered, the size of each determined by the cutoff mode N of the underlying Fourier series. A truncation to N positive Fourier modes reduces the exact bi-infinite system (11) to an approximate $(4N + 2)$-dimensional problem. For several choices of k and B, a value of $N = N(k, B)$ was chosen to ensure that the resulting eigenvalues had converged to within a measured tolerance. A simple polynomial was used to fit this data. This information, and details related to other parameter ranges used in the experiments, are included in Table 2. In the table, k is the elliptic modulus (3), B is the offset parameter and may be interpreted as a measure of the nontrivial-phase quantity θ, $(4N+2)$ is the matrix dimension used to approximate the full operator, ρ is the wavenumber of the perturbation in the y-dimension, and μ is the Floquet exponent. Lastly, $\texttt{linspace}(\texttt{a}, \texttt{b}, \texttt{m})$ is a linearly spaced vector from a to b of length m, $\texttt{logspace}(\texttt{a}, \texttt{b}, \texttt{m})$ is a logarithmically spaced vector from 10^a to 10^b of length m and `ceil(x)` is the smallest integer not less than x.

3.3 Observations

First and foremost, it should be stated that *none* of the NTP solutions considered here were found to be spectrally stable under one-dimensional ($\rho = 0$, *i.e.* longitudinal) or two-dimensional ($\rho \neq 0$) perturbations. This establishes, at least numerically, that *all* one-dimensional traveling-wave solutions of NLS of the form given by (2) are spectrally unstable with respect to both one- and two-dimensional perturbations. At this point, it remains to investigate the nature of the instabilities and their corresponding growth rates, so as to better understand the dynamics of this important class of solutions of the NLS equation.

Using Hill's method we numerically considered the instabilities due to perturbations with

wavenumber $\rho \in [0, 4]$. Note the $\rho = 0$ corresponds to one-dimensional, *i.e.* purely longitudinal, perturbations. For each NLS equation (*i.e.* for each choice of $\alpha, \beta = \pm 1$), and solution (*i.e.* each parameter pair (k, B)), and for each perturbation of wavenumber ρ, a sequence of a sequence of Floquet parameters μ was chosen from the interval $[-\frac{\pi}{K}, \frac{\pi}{K})$. The generalized eigenvalues and eigenvectors were computed the matrix that results from the truncated version of (11). The eigenvalues are approximations of spectral elements of (8), and an approximation of the corresponding eigenfunctions may be reconstructed from the eigenvectors.

Since a single eigenvalue with positive real part leads to instability of the system, the eigenvalue with largest real part over all choices of μ was recorded for each (k, B, ρ) triplet. That is, we compute

$$\Omega_{growth}(k, B, \rho) = \max_{\mu \in [-\pi/K, \pi/K]} Re\left[\Omega(k, B, \rho, \mu)\right], \tag{12}$$

which we call the (most unstable) growth rate. The constant Ω_{growth} represents the largest exponential growth rate a given NTP solution with parameters (k, B) will experience when perturbed with transverse wavenumber ρ. We reduce the dimension further by computing the largest such growth rate over all sampled perturbation wavenumbers ρ. This quantity,

$$\Omega_{\max}(k, B) = \max_{\rho \in [0,4]} \Omega_{growth}(k, B, \rho), \tag{13}$$

the maximal growth rate over all ρ, is plotted in the first columns of Figs. 2 and 3. The constant $\Omega_{\max}(k, B)$ represents the maximal exponential growth rate that a solution with parameters (k, B) can undergo in the range examined, and allows us to determine the perturbation to which the NTP solution is spectrally the most unstable. We also recorded the minimum growth rate over all ρ,

$$\Omega_{\min}(k, B) = \min_{\rho \in [0,4]} \Omega_{growth}(k, B, \rho), \tag{14}$$

to verify that all solutions are unstable with respect to every sampled perturbation.

Every point plotted in Figs. 2 and 3 corresponds to an NLS solution for which we computed the linear stability analysis, and the boundaries in the figures are the boundaries of the regions represented in Fig. 1 and correspond to limiting TP solutions. Fig. 2 corresponds to the x-focusing ($\alpha = 1$) parameter range $(k, B) = (0, 1) \times (2k^2, 2)$ in the $\alpha = 1$ case of Fig. 1(a). The one-to-one transform $T_f(B) = (B - 2k^2)/(2 - 2k^2)$ is used to normalize the range of B. This maps the interval $[2k^2, 2]$ to $[0, 1]$. Fig. 3 corresponds to the x-defocusing ($\alpha = -1$) parameter range of $(k, B) = (0, 1) \times (-1, 0)$ shown in Fig. 1(b). The transform $T_d(B) = -B$ is used in Fig. 3. A $\log_{10}$ scale is used in the vertical dimension of Figs. 2 and 3. This causes the panels of Fig. 2 to become increasing sparse in their lower right corners. The right-hand panels of Figs. 2 and 3 indicate the wavenumber ρ that leads to maximal growth shown in the left-hand panels. Recall that our computations were truncated at $\rho = 4$.

3.3.1 Case I: Elliptic setting with $\alpha = \beta = 1$

Panels Ia and Ib of Fig. 2 summarize some properties of the computed instabilities in the case of focusing in both the x- and y-dimensions. The lower boundary of the plot corresponds to $B = 2k^2 + (10^{-8})$, and is therefore only slightly away (in the parameter space of B) from a cn-type solution. The upper boundary is close to dn-type solutions, with $B = 1.99$. The left boundary of the plots, where $k = 0.01$, represents a region in parameter space near to Stokes' wave solutions.

The entire right-hand boundary, where $k = 0.99$, is near to the bright soliton limit case which occurs at $(k, B) = (1, 2)$.

A distinct ridge of large instability is noticeable in the plot of $\Omega_{\max}$ in panel Ia of Fig. 2. The ridge appears to begin near the zero solution at $(k, B) = (0, 0)$, and remains close to the cn limit boundary (within approximately .02 units) as k increases. Moving away from the cn boundary results in the rapid increase of $\Omega_{\max}$. Movement away from the dn boundary results in a much slower increase in the value of $\Omega_{\max}$, as does moving away from the Stokes' wave boundary for B larger than approximately 0.001. The maximum value of $\Omega_{\max}$ over the sampled (k, B) space, given by $R_{\max} = 5.666$, is reached near $(k, B) \approx (0.99, 1.98)$. The minimum ($R_{\min} = 0.015693$) occurs for $(k, B) \approx (0.01, 0.01)$ for $\rho = 4$. Since $\psi \equiv 0$ is a stable solution of the NLS equation, this minimum goes to zero as $(k, B) \to 0$.

In panel Ib, the wavelength corresponding to the maximal growth of Ia is given. In this case, the maximum instability occurs for the shortest wavelength samples, $\rho = 4$. This indicates that there is a strong short-wavelength instability.

3.3.2 Case II: Hyperbolic setting with $\alpha = -\beta = 1$

Panels IIa and IIb of Fig. 2 summarize some properties of the computed instabilities in the case of focusing in the x-dimension and defocusing in the y-dimension. The lower boundary of the plot corresponds to $B = 2k^2 + (10^{-8})$, and is therefore only slightly away (in the parameter space of B) from a cn-type solution. The upper boundary is close to dn-type solutions, with $B = 1.99$. The left boundary of the plots, where $k = 0.01$, represents a region in parameter space near to Stokes' wave solutions. The entire right-hand boundary, where $k = 0.99$, is near to the bright soliton limit case which occurs at $(k, B) = (1, 2)$.

As in Case I, a ridge of large growth rate is noticeable in the growth plot included in panel IIa. The ridge appears to begin near the zero solution at $(k, B) = (0, 0)$, and remains close to the cn-type limit boundary (within approximately .02 units) as k increases. This ridge has a local minimum near $k = 0.7$ and increases to a global (over all admissible (k, B)-parameter space) maximum near $k = 0.96$. As in the setting above, moving away from the cn-type boundary results in a rapid increase of $\Omega_{\max}$. Moving away from the dn boundary results in a much slower increase in the value of $\Omega_{\max}$. For $B > 0.001$, moving away from the boundary result in a similar slow increase in $\Omega_{\max}$. **For $k > 0.96$, the overall decrease in $\Omega_{\max}$ is consistent with stability results for the TP bright soliton limit [14].** The maximum ($R_{\max} = 6.1141$) and minimum ($R_{\min} = 0.012535$) growth rates span a slightly larger range than the similar values in Fig. 2. These are centered near $(k, B) \approx (0.01, 0.01)$ and $(k, B) \approx (0.96, 1.98)$, respectively.

In panel IIb, the wavelength corresponding to the maximal growth $R_{\max}$ of IIa are given. In this case, the maximum instability of R_{max} occurs for $\rho = 3.375$. The surface represented by IIb appears to be much smoother than the surface of Ib.

3.3.3 Case III: Hyperbolic setting with $-\alpha = \beta = 1$

Panels IIIa and IIIb of Fig. 3 summarize some properties of the computed instabilities in the case of defocusing in the x-dimension and focusing y-dimension. The lower limit of the plot corresponds to $B = -(10^{-8})$, and so is just slightly away from the sn-type solution. The left boundary of the plots, where $k = 0.01$, represents a region in parameter space near to Stokes' wave solutions, while $k = 0.99$ on the right boundary is near to the gray soliton limit.

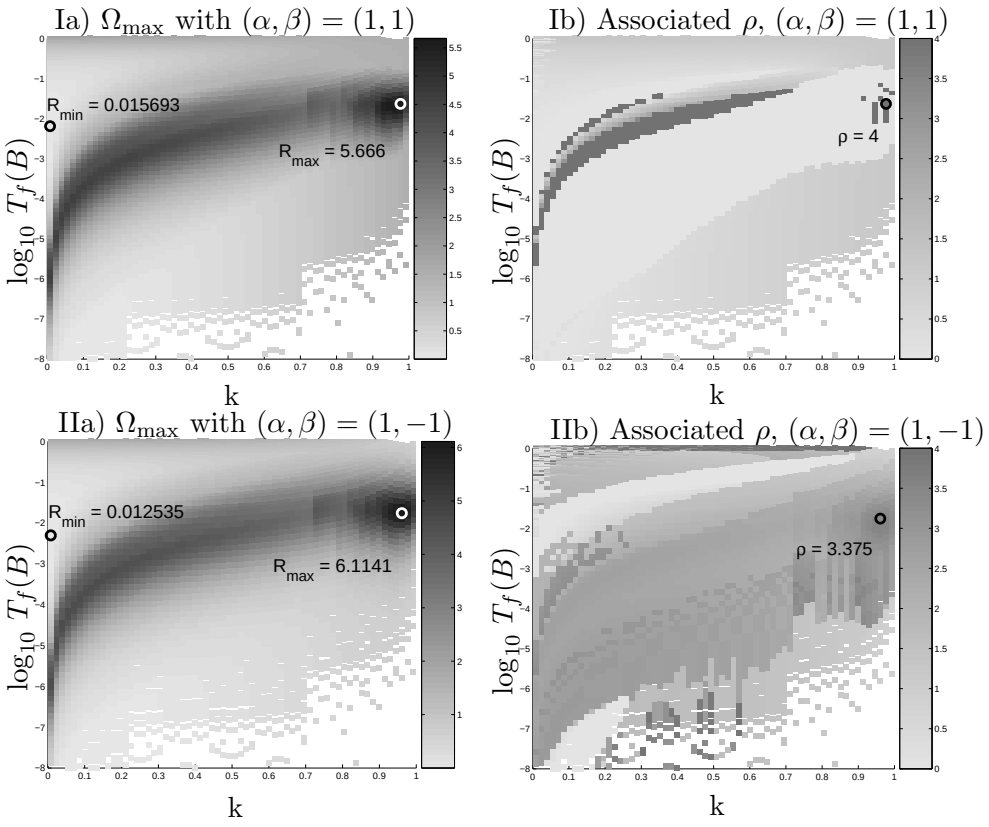

Figure 2: Focusing in the x-dimension. Here a) contains surface plots of $\Omega_{\max}$ vs. (k, B) and b) contains the surface plots of the wavenumber ρ corresponding to $\Omega_{\max}$ vs. (k, B). $\mathrm{R}_{\max} = \max_{k,B} \Omega_{\max}$ and $\mathrm{R}_{\min} = \min_{k,B} \Omega_{\min}$. White space corresponds to (k, B)-parameter space that was *not* sampled.

A distinct ridge of large instability is noticeable in the growth plot included in panel IIIa. The ridge appears to begin near the zero solution limit at $(k, B) = (0, 0)$, and remains close to the sn limit boundary (within approximately .02 units) as k increases. It quickly reaches the global maximum (over all admissible (k, B)-parameter space) of $R_{\max} = 7.6375$ near $k = 0.02$ and $B = -0.0001$. The ridge then appears to decrease in amplitude as k increases towards 1. Moving away from the sn-type boundary results in a rapid increase of $\Omega_{\max}$. Moving away from the dn-type boundary results in a much slower increase in the value of $\Omega_{\max}$. Similarly, there is much slower increase when moving away from the Stokes' wave limit for $B > 0.001$. The maximum exponential growth rate, $R_{\max} = 7.6375$, occurs for $(k, B) \approx (0.02, 0.00001)$. The minimum exponential growth, $R_{\min} = 0.015578$ is found near $(k, B) \approx (0.01, 0.9)$. Both the maximum and minimum are located near the Stokes' wave boundary. **By restricting $\rho = 0$ and allowing B to approach zero, $\Omega_{\max} \to 0$, and the stability result of the sn-type TP solution of [5] is recovered.**

The plot IIIa indicates short-wave perturbations lead to large values of $\Omega_{\max}$. The largest growth occurs for a perturbation with wavenumber of $\rho = 3.625$.

3.3.4 Case IV: Elliptic setting with $-\alpha = -\beta = 1$

Panels IVa and IVb of Fig. 3 summarize some properties of the computed instabilities in the case of defocusing in both the x- and y-dimensions. The lower limit of the plot corresponds to $B = -(10^{-8})$, and so is just slightly away from the sn-type solution. The left boundary of the plots, where $k = 0.01$, represents a region in parameter space near to Stokes' wave solutions, while $k = 0.99$ on the right boundary is near to the gray soliton limit.

A distinct ridge of large instability is noticeable in the growth plot included in panel IVa. The ridge appears to begin near the trivial limit $k = 0$ and $B = 0$, and remains close to the sn limit boundary (within approximately .02 units) as k increases, to reach a global maximum near $k = 0.02$ and $B = -0.0001$. The ridge then appears to decrease in amplitude as k increases towards 1. As in Case III, moving away from the sn-type boundary results in a rapid increase of $\Omega_{\max}$. Moving away from the dn-type boundary results in a much slower increase in the value of $\Omega_{\max}$. The same is true when moving away from the Stokes' boundary, when B is larger than approximately 0.001. The maximum exponential growth rate, $R_{\max} = 7.6456$, and the minimum, $R_{\min} = 0.0001556$, span a slightly larger range of values than do the values of $\Omega_{\max}$ in panel IIIa). The maximum and minimum values are obtained near $(k, B) \approx (0.01, 0.00009)$ and $(k, B) \approx (0.01, -1)$, respectively. Both are located near to the Stokes' wave boundary. **As in Case III, restricting $\rho = 0$ and allowing B to approach zero results in $\Omega_{\max} \to 0$, and the stability result of [5] for the sn-type TP solution is recovered.**

In panel IVb, wavenumbers corresponding to $\Omega_{\max}$ of IVa are given. It appears that a majority of the large values of $\Omega_{\max}$ are attributable to small ρ (long-wave) perturbations. In fact, the largest growth occurs for $\rho = 0$, the one-dimensional perturbation. In contrast, short-wavelength two-dimensional perturbations with wavenumber $\rho > 3$ were associated with many of the large $\Omega_{\max}$ values in the previous plots.

4 Summary

In this paper, we considered the spectral instability of one-dimensional traveling-wave nontrivial-phase (NTP) solutions of the cubic nonlinear Schrödinger equation. Such solutions are expressed in terms of Jacobi elliptic functions. An exact spectral form of the linearized operator is truncated and used to construct an associated generalized eigenvalue problem. The positive real parts of the resulting eigenvalues were used to determine that there are *no* spectrally stable NTP solutions.

Numerical results indicate a well-defined ridge of large growth rate located in the (k, B)-parameter region associated with fully nontrivial-phase solutions. This means that perturbed NTP solutions are more unstable than perturbed TP solutions, *i.e.* for a given transverse wavenumber ρ they exhibit larger exponential growth rates. **Also, the exponential growth rate $\Omega_{\max}$ increases quickly when moving away from the sn- and cn-type solutions, and increases much more slowly when moving away from the dn-type and Stokes' wave solutions. We interpret this to mean that solutions near to the sn- and cn-type solutions are sensitive to small changes in B. For a fixed k, stability of dn-type solutions are less sensitive to changes in B than the cn-type solutions. Near to the Stokes' wave, changes in k result in a relatively minor increase of $\Omega_{\max}$, as long as the initial solution is not close to the zero solution.**

In summary, numerical evidence suggests that all bounded, nontrivial-phase one-dimensional traveling-wave solutions to the cubic NLS equation are unstable with respect to both one-dimensional

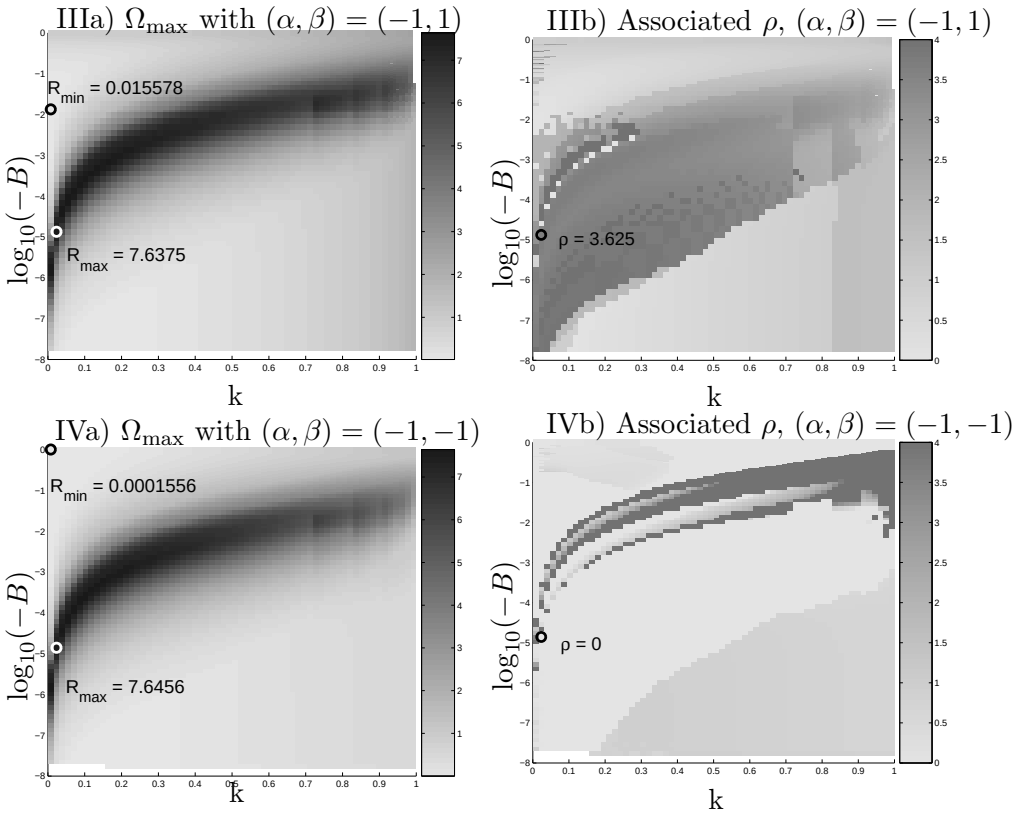

Figure 3: Defocusing in the x-dimension. Here a) contains surface plots of $\Omega_{\max}$ vs. (k, B) and b) contains surface plots of the ρ corresponding to $\Omega_{\max}$ vs. (k, B). $\mathrm{R}_{\max} = \max_{k,B} \Omega_{\max}$ and $\mathrm{R}_{\min} = \min_{k,B} \Omega_{\min}$.

(longitudinal) and two-dimensional perturbations.

The *National Science Foundation* is acknowledged for its support (NSF-DMS 0139093 and NSF-DMS 0139771).

References

[1] V. A. Aleshkevich, A. A. Egorov, Y. V. Kartashov, V. A. Vysloukh, and A. S. Zelenina. Stability of spatiotemporal cnoidal waves in cubic nonlinear media. *Phys. Rev. E*, 67:066605, 2003.

[2] P. F. Byrd and M. D. Friedman. *Handbook of Elliptic Integrals for Engineers and Physicists*. Springer-Verlag, Berlin, 1954.

[3] L. D. Carr, C. W. Clark, and W. P. Reinhardt. Stationary solutions of the one-dimensional nonlinear Schrödinger equation. I. Case of repulsive nonlinearity. *Phys. Rev.A*, 62:63610, 2000.

[4] L. D. Carr, C. W. Clark, and W. P. Reinhardt. Stationary solutions of the one-dimensional nonlinear Schrödinger equation. II. Case of attractive nonlinearity. *Phys. Rev.A*, 62:63611, 2000.

[5] J. D. Carter and B. Deconinck. Stability of trivial-phase solutions of the two-dimensional cubic nonlinear Schrödinger equation. *Submitted for publication*, 2005.

[6] J. D. Carter and H. Segur. Instability in the two-dimensional cubic nonlinear Schrödinger equation. *Phys. Rev. E.*, 68(4):045601, 2003.

[7] B. Deconinck and J. N. Kutz. Computing spectra of linear operators using Hill's method. *Submitted for publication*, 2005.

[8] B. Deconinck, D. E. Pelinovsky, and J.D. Carter. Transverse instabilities of deep-water solitary waves. *Submitted for publication*, 2005.

[9] S. E. Fil'chenkov, G. M. Fraiman, and A. D. Yunakovskii. Instability of periodic solutions of the nonlinear Schrödinger equation. *Sov. J. Plasma Phys.*, 18(8):961–966, 1987.

[10] G. H. Golub and C. F. Van Loan. *Matrix Computations*. Johns Hopkins University Press, Baltimore, MD, 1996.

[11] E. Infeld and J. Ziemkiewicz. Stability of complex solutions of the nonlinear Schrödinger equation. *Acta Phys. Pol.*, A59(3):255–275, 1981.

[12] C.G. Jacobi. *Gessammel Werke*. Königsberg, 1829.

[13] Y. V. Kartashov, V.A. Aleshkevich, V.A. Vysloukh, A.A. Egorov, and A.S. Zelenina. Transverse modulational instability of (2+1)-dimensional cnoidal waves in media with cubic nonlinearity. *J. Opt. Soc. Am. B.*, 20(6):1273–1284, 2003.

[14] Y. S. Kivshar and D. E. Pelinovsky. Self-focusing and transverse instabilities of solitary waves. *Phys. Rep.*, 331(4):118–195, 2000.

[15] E.A. Kuznetsov, A.M. Rubenchik, and V.E. Zakharov. Soliton stability in plasmas and hydrodynamics. *Phys. Rep.*, 142:103–165, 1986.

[16] D. U. Martin, H. C. Yuen, and P. G. Saffman. Stability of plane wave solutions of the two-space-dimensional nonlinear Schrödinger equation. *Wave Motion*, 2:215–229, 1980.

[17] K. Rypdal and J. J. Rasmussen. Stability of solitary structures in the nonlinear Schrödinger equation. *Phys. Scripta*, 40:192, 1989.

[18] P. L. Sulem and C. Sulem. *Nonlinear Schrödinger Equations: Self-focusing and Wave Collapse.* Springer-Verlag, New York, NY, 1999.

[19] V. E. Zakharov and A. M. Rubenchik. Instability of waveguides and soliton in nonlinear media. *Sov. Phys. JETP*, 38(3):494–500, 1974.